Journal of Electroanalytical Chemistry 995 (2025) 119324

Contents lists available at ScienceDirect

Journal of Electroanalytical Chemistry

journal homepage: www.elsevier.com/locate/jelechem

Searching bioalcohols for more sustainable fuel cells: On the electrochemical oxidation of a glycerol platform molecule on gold

Dalila S. Mekazni [a,b], Antonio Rodes [a], Rosa M. Arán-Ais [a], Alejandro Leal-Duaso [b,c,*], Carlos M. Sánchez-Sánchez [b], Enrique Herrero [a,**]

[a] Instituto de Electroquímica, Universidad de Alicante, Apdo. 99, E-03080 Alicante, Spain
[b] Sorbonne Université, CNRS, Laboratoire Interfaces et Systèmes Electrochimiques (LISE), 4 place Jussieu, F-75005 Paris, France
[c] Universidad de Zaragoza (Programa Margarita Salas), ISQCH-CSIC, calle Pedro Cerbuna, E-50009 Zaragoza, Spain

ARTICLE INFO

Keywords:
Glycerol
Glycidol
Electrooxidation
Bio-based fuels
Gold electrodes
FTIR spectroscopy

ABSTRACT

In this work, the electrochemical oxidation of a bio-based platform molecule derived from glycerol, namely glycidol, was investigated on gold electrodes and compared to the electrooxidation of glycerol, since both are C_3-based alcohols derived from the same renewable biomass source. Cyclic voltammetry, chronoamperometry, and in situ Fourier-transform infrared spectroscopy (FTIR) experiments were performed in alkaline and acidic media at room temperature to analyze reaction mechanisms and products formation. Both glycerol and glycidol exhibited high reactivity in alkaline conditions. Nevertheless, glycerol oxidation on gold electrodes showed higher activity than glycidol, which can be attributed to the highly stable cyclic structure of glycidol and differences in the acidity of their alcohol groups. FTIR analysis and in situ infrared reflection absorption spectroscopy of glycidol electrooxidation revealed the formation of various carboxylate anions and also carbonate, indicating that in some cases the complete cleavage of the C—C bond has taken place. These findings provide valuable insights into the electrochemical behavior of glycerol-derived molecules on gold, contributing to the development of more sustainable bio-based fuels.

1. Introduction

Over the last decades, fuel cells (FC) have emerged as one of the most promising energy conversion technologies [1–3]. As the demand for efficient and sustainable power sources continues to grow, fuel cells are expected to play a crucial role in the transition to green energy [4]. The electrochemical oxidation of organic molecules presents a great interest in electrocatalysis [5,6], not only from a fundamental perspective, but also due to its relevance in anodic processes for FC applications [7–11]. In this context, alcohols have gained significant attention for Direct Alcohol Fuel Cells (DAFCs) due to their high energy density, as well as their ease of storage and handling [12–16]. However, beyond the technical and performance aspects of DAFCs, the sustainability of the fuel source must also be considered. The viability of alcohol-based fuels depends on their renewable origin and widespread availability, ensuring long-term accessibility and minimal environmental impact [4,17].

Glycerol, a C_3-polyol with three hydroxyl functional groups, is widely used in food, pharmaceutical, and chemical industries [18]. Currently, the primary source of glycerol is the production of biodiesel through biomass esterification, where it is generated as a major byproduct accounting for up to 90 % of the total weight of products. Despite its extensive industrial applications, the global glycerol production has consistently exceeded demand since 2000, leading to a growing surplus [19]. All these facts convert glycerol into one of the most easily available renewable materials at present [20]. To address this surplus, a number of various glycerol derivatives have been developed and applied across different sectors [19,21]. Among them, glycerol-derived molecule platforms, including glycidol, epichlorohydrin and glycerol carbonate (see Fig. 1), offer a versatile approach to glycerol valorization, while overcoming some of its inherent drawbacks [22–24]. Compared to glycerol, these derivatives exhibit lower viscosity, lower hydrophilicity, and higher volatility, allowing for improved control over reaction selectivity, when used in a chemical reaction [25–27]. Additionally, sustainable synthetic routes from bioglycerol to these compounds are already industrially available [23]. Finally, it is important to highlight that both glycerol and, in general, its derived

* Corresponding author at: Sorbonne Université, CNRS, Laboratoire Interfaces et Systèmes Electrochimiques (LISE), 4 place Jussieu, F-75005 Paris, France.
** Corresponding author.
E-mail addresses: alduaso@unizar.es (A. Leal-Duaso), herrero@ua.es (E. Herrero).

https://doi.org/10.1016/j.jelechem.2025.119324
Received 21 April 2025; Received in revised form 26 June 2025; Accepted 3 July 2025
Available online 5 July 2025

molecules possess minimal ecotoxicity and low environmental impact [28], making them promising candidates for fuel cell applications.

Glycerol electrooxidation reaction (GEOR) has been very recently proposed as a promising strategy for both glycerol valorization and clean energy generation, not only in DAFCs but also in the electrochemical production of hydrogen by replacing the more energy-demanding oxygen evolution reaction [29–31]. In the electrooxidation of alcohols, the electrode material plays a crucial role, as a highly efficient electrocatalyst is required to enhance the performance. Over the last decade, extensive research has focused on controlling the GEOR selectivity, with several noble metal electrocatalysts —including platinum, palladium, silver, and gold— showing varying degrees of efficiency [32–35]. Among all these noble metals, gold has demonstrated a superior catalytic activity for glycerol electrooxidation, offering higher selectivity and efficiency for its valorization, as well as less sensitivity towards deactivating chemisorption of oxidation intermediates such as carbon monoxide [36–38]. However, the electrochemical oxidation of other glycerol derivatives, such as glycidol or glycerol carbonate, remains unexplored today.

As described in Eq. (1), the complete oxidation of glycerol to CO_2 requires the exchange of 14 electrons through a complex, multi-step mechanism [39]. This process involves adsorption of glycerol, multiple electron transfers, interaction with oxygenated species, and final desorption of oxidation products. All these steps, and especially for the case of gold, are highly sensitive to the experimental conditions, including surface structure and electrolyte composition, which significantly impact both reaction efficiency and product selectivity [40]. In contrast, no mechanism has been proposed so far for the electrooxidation of any glycerol derivative, including glycidol. Complete oxidation of glycidol to CO_2 also would require the exchange of 14 electrons, as described in Eq. (2).

$$C_3H_8O_3 + 14\ OH^- \rightleftharpoons 3\ CO_2 + 11\ H_2O + 14\ e^- \quad (1)$$

$$C_3H_6O_2 + 14\ OH^- \rightleftharpoons 3\ CO_2 + 10\ H_2O + 14\ e^- \quad (2)$$

In this work, the performance and mechanism of the electrochemical oxidation of glycerol and glycidol on bulk gold electrodes and supported gold nanoparticles have been studied and compared, in both acidic and alkaline media, by means of cyclic voltammetry, chronoamperometry, and in situ FTIR experiments, thus contributing to the valorization of renewable glycerol and its derivatives, as well as to the development of more sustainable anodic processes for energy and electrocatalytic applications.

2. Experimental section

The working electrodes used in this study were either a gold disc or gold nanoparticles supported on a glassy carbon (GC) electrode. The gold disc electrode (CH Instruments 101) presents a geometric area of 0.0314 cm^2. Gold nanoparticles supported on carbon (Metrohm, 99.99 %) were deposited on a GC disc electrode (CH Instruments 104) with a geometric area of 0.0707 cm^2. Prior to each experiment, both gold and GC disc electrodes were mechanically polished with alumina powder (0.05 μm) for 3 min, rinsed with ultrapure water, and sonicated in order to remove any remaining particles from previous experiments. The supported gold nanoparticles were deposited over the abovedescribed GC disc by placing 20 μL of the nanoparticles' aqueous suspension (concentration 20 mg L^{-1}, loading mass $4{\cdot}10^{-4}$ mg), and dried under argon flow (Alphagaz, 99.995 %). The morphology of the gold nanoparticles was characterized using a SEM-FEG Ultra55 scanning electron microscope (SEM) from Carl Zeiss. The size of the gold nanoparticles was evaluated with a JEOL 2011 transmission electron microscope (TEM) from JEOL.

All chemicals used were of analytical grade. Glycerol (≥99.5 %), glycidol (96 %), and glycerol carbonate (99 %) were purchased from Sigma-Aldrich. The working solutions were prepared using MilliQ ultrapure water (Purelab Flex, 18.2 MΩ cm) and contained either 0.10 M NaOH (Fisher Chemicals, ≥98 %) or 0.10 M $HClO_4$ (Sigma-Aldrich, >99 %) as the supporting electrolyte, together with different concentrations of glycerol (Sigma-Aldrich, ≥99.5 %) or glycidol (Sigma-Aldrich, 96 %).

All electrochemical experiments were carried out in a conventional three-electrode glass cell. A graphite rod (diameter 3.05 mm, Thermo Scientific 99.9995 %) and an Ag/AgCl electrode (in 3 M KCl solution) were used as the counter and reference electrodes. For better comparison between experiments at different pH values, all the potentials have been reported vs. the reversible hydrogen electrode (RHE). Cyclic voltammograms were recorded using a CH Instruments 760 (CHI 760) potentiostat, typically at 50 mV s^{-1}. All the experiments were carried out at room temperature. In all experiments (using both gold disc and supported gold nanoparticles), current densities have been normalized by the geometrical surface area of the gold electrode.

Attenuated total reflection absorbance infrared (ATR-FTIR) spectra for glycidol and the possible reaction products were recorded using a Nexus8700 spectrometer from Thermo Scientific equipped with an MCT-A detector. The measurements were performed using a ZnSe prism bevelled at 45° with a resolution of 8 cm^{-1}, averaging 20 interferograms per spectrum. These spectra were referred either to that collected under the same conditions for pure water or that for an aqueous sodium hydroxide solution. In situ infrared reflection absorption spectroscopy (IRRAS) experiments were carried out using a Nicolet iS50 FTIR spectrometer equipped with a narrow-band DC-coupled MCT-A detector. The spectroelectrochemical cell had a prismatic CaF_2 window bevelled at 60°. The experiments were carried out at room temperature. A RHE electrode and a gold wire were used as the reference and counter electrodes, respectively. The IR spectra were collected with p- or s-polarized light and with a resolution of 8 cm^{-1}. Single-beam infrared spectra were recorded during a linear potential scan at 2 mV s^{-1} in the range from 0.10 to 1.30 V. To increase the signal-to-noise ratio, 114 interferograms were co-added for the obtaining of each spectrum, which corresponds to a potential interval of 0.02 V. The spectra are depicted as the ratio –log (R_2/R_1), where R_2 and R_1 represent the single-beam sample and reference reflectance spectra, respectively. In this way, positive bands in the spectra correspond to species formed at the sampling potential, whereas negative bands indicate species consumed relative to the reference potential, which was selected at 0.10 V (i.e., well below the onset for glycidol electrooxidation).

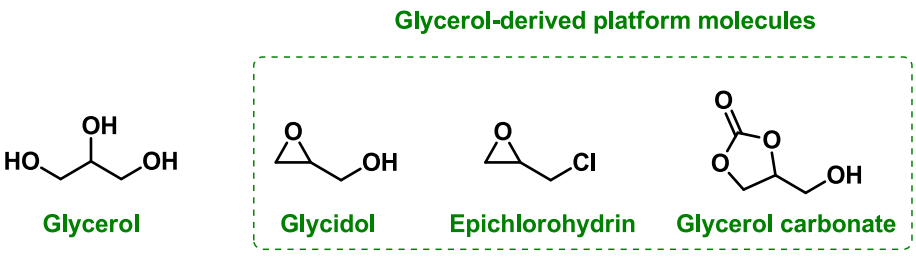

Fig. 1. Structure of glycerol and glycerol-derived platform molecules.

3. Results and discussion

3.1. Cyclic voltammograms of glycidol and glycerol oxidation on Au electrodes

To investigate the activity of the aforementioned alcohols to be electrochemically oxidized as possible bio-based fuel candidates, glycerol and its derived platform molecule, glycidol, were selected for this study (Fig. 1). Glycerol carbonate, another typical platform molecule from glycerol, was discarded as a fuel candidate from the beginning of this study due to its high chemical stability against oxidation. Like glycidol, glycerol carbonate contains an alcohol functional group susceptible to be oxidized to aldehyde and carboxyl groups. However, the increased stability of the carbonate ring likely hinders notably its oxidation.

Therefore, the electrochemical oxidation of those two bio-alcohols was initially investigated on a gold disc electrode using cyclic voltammetry at different pH conditions. Fig. 2 presents the cyclic voltammograms for the oxidation of glycerol and glycidol in strong alkaline (2a) and acidic (2b) media at a concentration of 0.1 M.

As shown in Fig. 2, both molecules exhibit significantly lower reactivity in acidic media (2b) compared to alkaline media (2a). In alkaline conditions, the onset potential for glycerol oxidation appears at approximately 0.70 V vs. RHE, while glycidol oxidation begins at *ca.* 0.85 V vs. RHE, indicating that glycerol is a priori more reactive. Following its onset potential, the current for glycerol oxidation increases linearly, reaching a maximum at 1.13 V, which coincides with the onset of gold oxide formation (dashed vertical line in Fig. 2(a)). Beyond this potential, the current decreases due to the formation of an oxide/hydroxide layer on the gold electrode. During the backwards scan, the current increases again as the oxide layer is reduced, achieving a secondary maximum for glycerol oxidation at ca. 1.30 V vs. RHE. However, due to the irreversible oxidation/reduction processes undergone by the gold surface, the currents observed in the backwards scan are lower than those shown in the forward scan.

For the case of glycidol oxidation, the onset potential is higher than that of glycerol, indicating lower reactivity as previously discussed. The current initially increases in a similar manner to glycerol oxidation, reaching a maximum at 1.20 V vs. RHE before gradually decreasing up to 1.40 V. This current decay demonstrates that the formed gold oxide is inactive for the oxidation of glycidol as is also the case for glycerol. During the reverse scan, no electrooxidation activity is observed between 1.40 and 1.20 V. Nevertheless, a sharp increase in oxidation current occurs at *ca.* 1.10 V, coinciding with the reduction of surface gold oxides back to metallic gold, which reactivates the glycidol electrooxidation. Notably, the decay in oxidation current is more pronounced for glycidol, and the reactivation of the surface due to oxide reduction occurs at a lower potential, close to the oxide reduction potential in the blank voltammogram. These differences suggest that the oxidation of these species influences the OH adlayer. In the case of glycerol, the likely participation of adsorbed OH in the oxidation mechanism results in lower OH coverages and delayed surface oxidation [37]. In contrast, for glycidol, the lower observed oxidation currents lead to a lesser impact on both the OH coverage and the gold oxide formation.

It is noteworthy to remark that the experimental current densities for glycerol oxidation in alkaline media are comparable to, or even exceed, those reported in the literature for palladium, platinum, and other gold-based catalysts [41,42]. More interestingly, while both alcohols exhibit a similar reactivity in acidic media, under alkaline conditions, the current density for glycerol oxidation is approximately three times higher than that of glycidol oxidation.

These observed differences in reactivity between acidic and alkaline media for the two alcohols can be attributed to differences in their oxidation mechanisms. It should be noted that in the oxidation of alcohols, the first step is always the adsorption of the molecule through the oxygen atom of the alcohol group [43,44]. Koper et al. reported that, in strongly alkaline media, the initial deprotonation of the alcohol is catalyzed by the base, rather than the metal surface [45]. Consequently, the main reactive species in glycerol oxidation is glycerolate, formed by the initial deprotonation of the α-hydroxy group. Oxidation then proceeds via the deprotonation of the β-hydroxy group, which has been identified as the rate-determining step in glycerol oxidation on gold [46]. In contrast, glycidol contains only one α hydroxyl group, which is significantly less acidic than the hydroxyl groups in glycerol [25]. As a result, the deprotonation step that initiates oxidation is considerably more difficult for glycidol than for glycerol, explaining the lower reactivity observed in Fig. 2(a). Indeed, the experimental glycerol pK_a value is 14.15, which is 2.8 times less acidic than the estimated glycidol pK_a, thus keeping the same proportion as the oxidation current densities

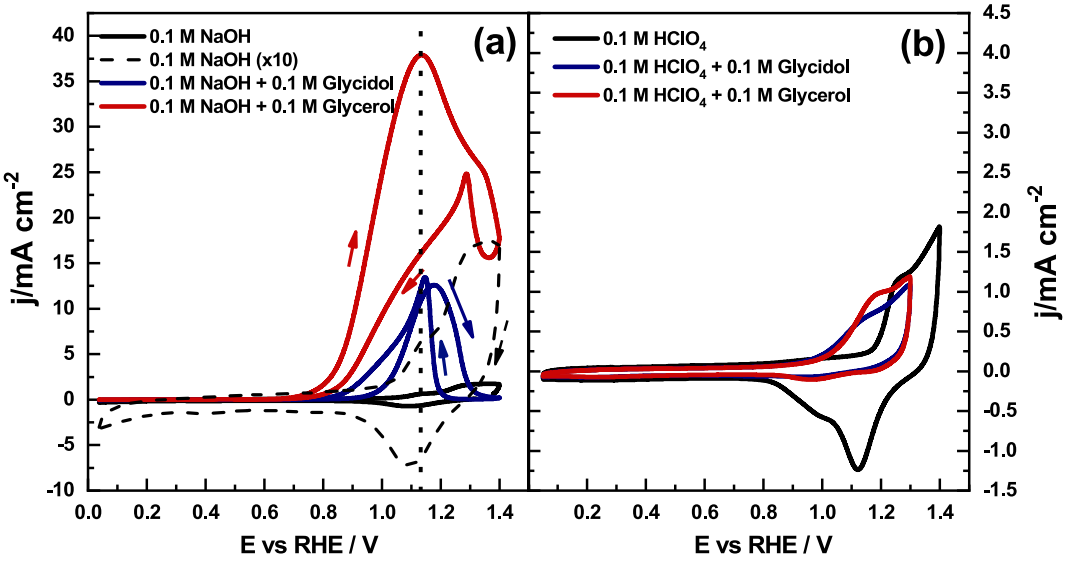

Fig. 2. Cyclic voltammograms of 0.1 M glycidol (blue line), 0.1 M glycerol (red line), and in the absence of any alcohol (black line) on a gold disc electrode in 0.1 M NaOH (a) and 0.1 M $HClO_4$ (b). Scan rate 50 mV s^{-1}. The dashed line in the (a) panel shows a 10-times enlargement of the curve in absence of alcohols. The dotted line indicates the onset potential for gold oxide formation. (For interpretation of the references to colour in this figure legend, the reader is referred to the web version of this article.)

difference between glycerol and glycidol. In the case of glycerol and glycidol oxidation in acidic media, the acidity of the substrate hydroxyl groups does not seem to play any role in the oxidation mechanism.

The effect of the scan rate on the electrooxidation of glycerol and glycidol was investigated under alkaline conditions to determine whether diffusion of reactants was affecting the oxidation currents. Fig. 3(a) presents the cyclic voltammograms for the oxidation of 0.1 M glycerol (Fig. 3(a1)) and 0.1 M glycidol (Fig. 3(a2)) on a gold disc electrode, recorded at scan rates ranging from 10 mV s^{-1} to 200 mV s^{-1}. As observed, the oxidation peak current increases with increasing the scan rate, accompanied by a shift in peak potential to higher values.

To determine the rate-controlling step of the reaction, the peak current was plotted against $v^{1/2}$. As shown in Fig. 3(b), a quasi linear relationship is observed between the anodic peak current and $v^{1/2}$ for both alcohols, indicating that the studied irreversible electrooxidation reactions are diffusion-controlled. For glycerol oxidation, the voltammetric profile exhibits characteristics typical of an irreversible process controlled by diffusion with a current decay beyond the peak current following the Fick's law. It should be highlighted that these voltammetric profiles already provides insight into the interplay between kinetics and mass transport. As shown in Fig. 3(a1) for glycerol oxidation, the rising part of the forward scan displays overlapping currents across different scan rates, indicating a kinetically limited regime where diffusion does not control the rates. After the oxidation peak, the current drops due to surface passivation by the formation of gold oxide. This process is slow and thus, depending on the scan rate, the oxide coverage is different. The extent of the surface oxidation at the upper potential affects the reactivity observed in the reverse scan. At scan rates below 50 mV s^{-1}, voltammograms overlap, and thus currents are controlled by the kinetics. At higher scan rates, partial oxidation occurs, and the current becomes scan-rate-dependent, reflecting mixed kinetic and mass transport control.

In contrast, for glycidol oxidation, the observed currents are smaller, and it is likely, based on the peak symmetry, that adsorption steps also influence the reactivity, contributing to a more complex oxidation mechanism.

In addition to gold disc electrodes, the electrooxidation of glycidol and glycerol was also studied and compared using polycrystalline gold nanoparticles (Au NPs) supported on carbon and deposited on a GC electrode. Electron microscopy analysis of these supported nanoparticles showed a typical average size of 40–70 nm (Fig. 4(b) and (c)). Fig. 4(a) presents the characteristic voltammetric profiles for both studied bioalcohols in 0.1 M NaOH solution. When using the supported gold nanoparticles in alkaline medium, the difference in reactivity between glycerol and glycidol became significantly more pronounced compared to the gold disc electrode. Although glycidol exhibited a more favorable oxidation peak potential (less positive, at 1.21 V vs. RHE), the sharp oxidation peak at over 1.30 V in the forward scan of glycerol indicates a much higher reactivity for glycerol oxidation compared to glycidol. These differences can be attributed to the porous nature of the nanoparticle-modified electrode. During the oxidation of both molecules, several intermediate products are formed. On a planar electrode, these intermediates diffuse away from the surface, whereas on a porous nanoparticulated Au electrode, they can be retained within the structure and undergo further oxidation. The greater relative increase in current for glycerol under these conditions suggests that its intermediate

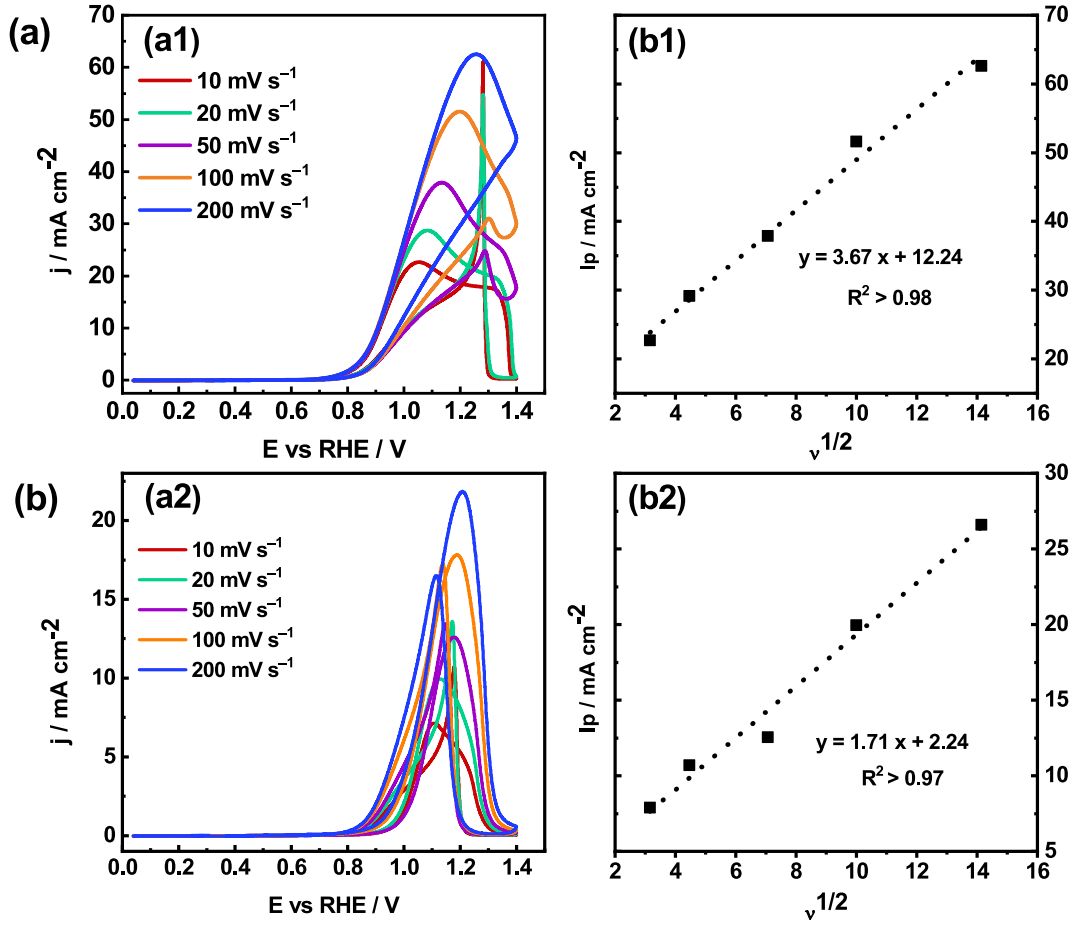

Fig. 3. (a) Cyclic voltammograms of 0.1 M glycerol (a1) and 0.1 M glycidol (a2) oxidation in 0.1 M NaOH on gold disc electrode at different scan rates. (b) Plots of anodic peak currents for glycerol (b1) and glycidol (b2) oxidation vs. the square root of the potential scan rate. (For interpretation of the references to colour in this figure legend, the reader is referred to the web version of this article.)

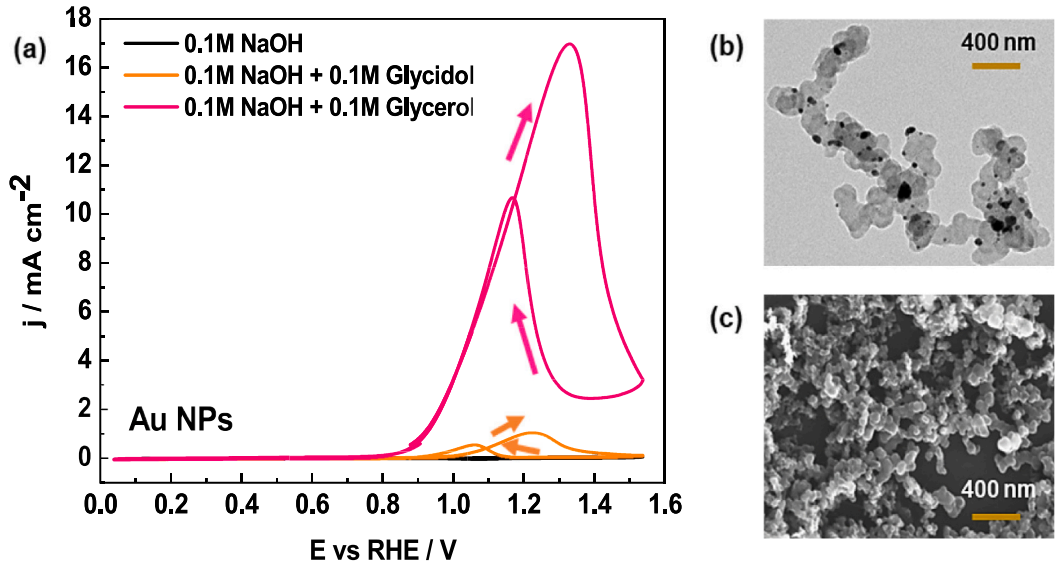

Fig. 4. (a) Cyclic voltammograms of glycerol and glycidol electrooxidation on Au polycrystalline nanoparticles supported on GC in 0.1 M NaOH solution. Scan rate 50 mV s^{-1}. (b) TEM and (c) SEM images of the supported Au NPs.

oxidation products are more readily oxidized than those of glycidol, which means that both alcohols do not share the exact same intermediates during electrooxidation. Interestingly, the difference in the potential required for reducing the gold oxide layer in the reverse scan remains unchanged on Au NPs.

Finally, the electrooxidation of glycerol and glycidol was also studied by chronoamperometric experiments on a gold disc electrode in alkaline solution (Fig. 5). Interestingly, no electrooxidation activity is observed for glycidol at 1.20 V and 1.30 V vs. RHE (red plots), due to inhibition provoked by the formation of gold oxides at the mentioned potentials, but significant activity is still observed for glycerol, particularly at 1.20 V (black plots). This would confirm that the formation of gold oxide is retarded in the presence of glycerol, as previously described by cyclic voltammetry in Fig. 2(a). Nevertheless, both alcohols exhibit significant electrooxidation activity at 1.00 V, with small progressive decays.

3.2. ATR-IR spectra of glycidol in solution and its possible oxidation products

To identify, for the first time, the products formed during the electrooxidation of glycidol on gold electrodes, ATR-IR spectroscopy was employed to analyze both glycidol in solution and its potential oxidation products. As shown in Fig. 6, ATR-IR spectra were recorded for two glycidol concentrations, 0.10 M (black line) and 0.50 M (red line), to assess concentration-dependent spectral variations and to ensure the detection of key functional groups involved in the oxidation process. The recorded spectra exhibit negative absorption bands corresponding to the characteristic vibrational modes of water, including O—H stretching (ν(OH)) at 3600–3000 cm^{-1} and H–O–H bending (δ(HOH)) at 1616 cm^{-1}. These bands increase in intensity as the glycidol concentration increases, indicating a rearrangement of bulk water molecules in the glycidol-containing solution due to molecular interactions with glycidol. A small band at 2900 cm^{-1} and a medium band at 905 cm^{-1} are assigned to ν(C—H) and δ(epoxy) modes of glycidol, respectively [47]. Additionally, a small band at 1262 cm^{-1} corresponds to the δ(CH_2) mode, while the most prominent absorption peak, appearing at 1040 cm^{-1}, is attributed to the ν(CO) mode of the α-alcohol group. A small band at 1105 cm^{-1} is commonly associated with ν(C—O) stretching in alcohols, whereas the band at *ca.* 959 cm^{-1} is assigned to the δ(CH) mode of aldehydes [48].

To further characterize the possible oxidation products formed during glycidol electrooxidation on gold electrodes, ATR-IR spectra of the salts of several reference organic acids were recorded. These salts include sodium oxalate, sodium acetate, sodium formate, and sodium glycolate. Note that the latter was obtained by dissolving glycolic acid in a concentrated sodium hydroxide solution. Also, the spectrum for glycolic acid in water was also included in the study. The spectra of all these compounds, gathered in Fig. 7, were analyzed to compare key vibrational features with those observed in glycidol oxidation. Notably, the absorption bands between 1300 cm^{-1} and 1600 cm^{-1}, attributed to

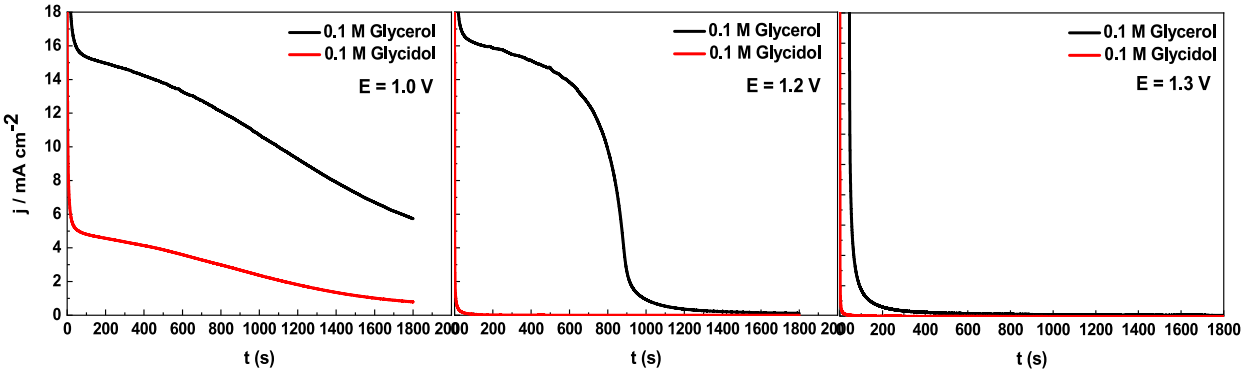

Fig. 5. Chronoamperometric profiles of 0.1 M glycerol (black lines) and 0.1 M glycidol (red lines) on gold disc electrode in 0.1 M NaOH solution at different applied potentials. (For interpretation of the references to colour in this figure legend, the reader is referred to the web version of this article.)

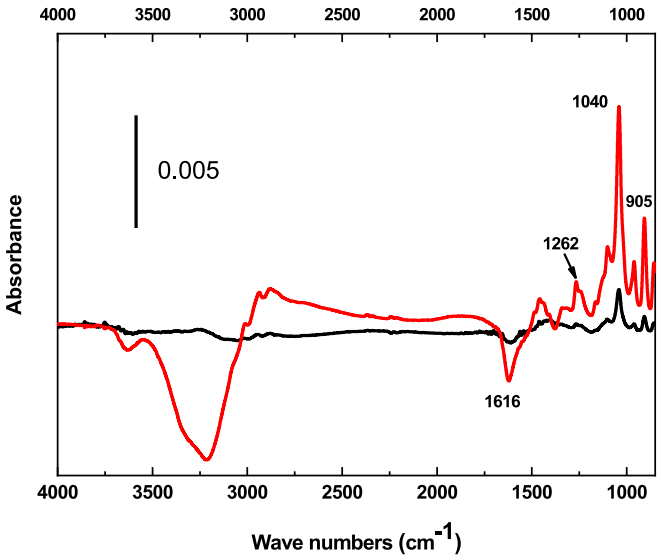

Fig. 6. ATR-IR absorbance spectra of 0.10 M (black line) and 0.50 M (red line) glycidol aqueous solution. Pure water was used as the background spectrum, details can be found in experimental section. (For interpretation of the references to colour in this figure legend, the reader is referred to the web version of this article.)

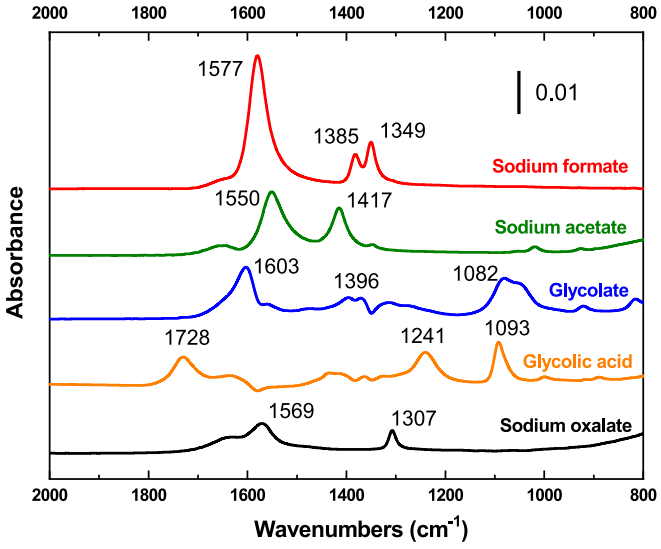

Fig. 7. ATR-IR absorbance spectra of aqueous 0.50 M solutions of sodium oxalate, glycolic acid, sodium glycolate, sodium acetate, and sodium formate.

O—C—O stretching (ν(OCO)) vibrations in carboxylates, exhibit distinct shifts and relative intensities, depending on the molecular structure of the corresponding salt. These variations allow for the differentiation of specific oxidation products and provide insights into the selectivity of glycidol oxidation pathways on gold electrodes. For instance, ATR-IR spectrum of the glycolic acid solution shows a characteristic band at *ca.* 1726 cm^{-1} that can be ascribed to the C—O stretching of the carbonyl group. Besides, additional bands are observed at *ca.* 1430 and 1242 cm^{-1}, which can be related to the C—(OH) stretching and OH bending modes of the carboxylic group [49]. Finally, mentioning that the spectra for glycolic acid and glycolate anion shares a common feature at *ca.* 1090 cm^{-1} that can be assigned to a combination of the OH stretching and bending modes of the hydroxymethyl moiety [50].

3.3. IRRAS spectra of glycidol-Au(polycrystalline) in alkaline medium

The electrooxidation of glycidol on polycrystalline gold surfaces in alkaline media was also investigated using in situ infrared reflection absorption spectroscopy (IRRAS) experiments. The aim was to identify reaction intermediates and oxidation products formed during the electrochemical oxidation process. Fig. 8(a) presents, in the wavenumber range of 1100–2500 cm^{-1}, a selection of the IRRAS spectra collected during a slow potential scan from 0.1 to 1.3 V (see the experimental section for details). Note that all these spectra are referred to the single beam spectrum recorded at 0.1 V in order to highlight spectral changes associated with the oxidation of glycidol at increasing potentials.

Before reaching the oxidation onset potential, which is approximately 0.80 V, specific absorption bands can already be identified in the spectra. In particular, bands appearing at 1547 cm^{-1} and 1430 cm^{-1} can be respectively attributed to the asymmetric and symmetric stretching vibrations of the carboxylate functional group. The exact frequency of these bands depends on the molecular structure of the different carboxylate species, which allows for the identification of different products based on the corresponding carboxylic acids (see the ATR-IR spectra shown in Fig. 7). In fact, the presence of these bands suggests that glycidol interacts with the gold surface, even before the epoxy ring is cleaved, leading to the formation of oxidation products. This initial interaction between glycidol and the electrode surface may play an important role in directing the oxidation pathway by stabilizing reaction intermediates prior to full electrooxidation.

Upon surpassing the oxidation onset potential, new absorption bands become visible in the spectra, indicating the formation of oxidation products. A sharp and intense band appears at 1590 cm^{-1}, which grows in intensity as the applied potential increases. Based on the precise position of this 1590 cm^{-1} band, it can be reliably assigned to the formation of formate by oxidation of glycidol. This assignment is also consistent with the observation of the corresponding symmetric stretching band at *ca.* 1329 cm^{-1} (see Fig. 7).

As the potential is further increased, up to a maximum at 1.30 V, an additional spectral feature emerges in the form of a new absorption band at 2343 cm^{-1}. This sharp band is indicative of the formation of CO_2, suggesting that some of the oxidation products undergo complete mineralization at higher potentials. The observation of CO_2 production implies that, due to the thin-layer configuration used in the experiment and the consumption of hydroxide ions during the oxidation process, the local pH at the electrode–electrolyte interface has significantly decreased. This local acidification effect has been experimentally verified as in similar electrochemical systems, and it plays a crucial role in the determination of the final oxidation products formed during glycidol electrooxidation. In this line, the hydrolysis of carbon dioxide to form some amount of carbonate and bicarbonate anions also contributes to the absorption bands appearing at around 1400 cm^{-1} [51].

Another significant spectral change occurs with the appearance of a shoulder at around 1730 cm^{-1} in the spectra reported in Fig. 8, which could be ascribed to the carbonyl group of glycolic acid. Another band corresponding to this formed species, appearing in Fig. 7 at around 1430 cm^{-1}, overlaps with the symmetric O—C—O stretching vibration of carboxylate anions, whereas those observed at 1242 cm^{-1} and 1099 cm^{-1} could be below the detection limit in the in situ experiments. As discussed above for carbon dioxide, the detection of acidic species can be justified as an effect of the consumption of hydroxide ions associated to the glycidol oxidation, which causes a significant decrease of the solution pH in the thin solution layer between the electrode surface and the infrared window. Glycolic acid is known to be a key intermediate in the alkaline electrooxidation of glycerol, which shares important structural similarities with glycidol [37,52]. The appearance of these bands supports the idea that glycidol follows an oxidation pathway that involves cleavage of its carbon–carbon bonds, leading to the generation of multiple oxidation intermediates, most of which are carboxylate-containing species as has been demonstrated above.

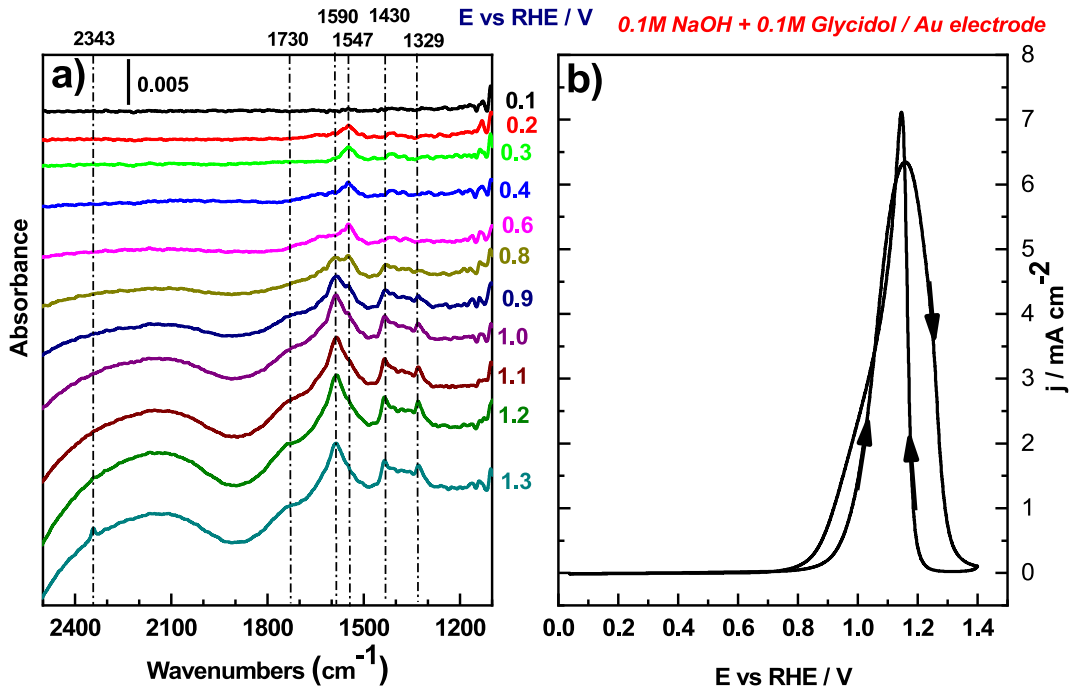

Fig. 8. (a) In situ IRRAS spectra (p-polarization) for the electrooxidation of glycidol on a gold disc electrode in 0.10 M (aqueous) NaOH +0.10 M glycidol. (b) Cyclic voltammogram of gold electrode in 0.10 M NaOH +0.10 M glycidol. (For interpretation of the references to colour in this figure legend, the reader is referred to the web version of this article.)

To further investigate whether the detected species were present in solution or remained adsorbed on the electrode surface, additional IRRAS spectra were recorded using different polarization modes. By using s- or p-polarized light, the interaction of glycidol and its oxidation products with the gold surface could be assessed. The resulting spectra, gathered in Fig. 9, show no significant differences between the two polarization modes, indicating that all detected species are present in solution rather than being strongly adsorbed onto the electrode surface. This finding suggests that the oxidation intermediates and products formed during glycidol electrooxidation are largely soluble and do not accumulate on the gold surface, which may have positive implications for the long-term stability and efficiency of the electrooxidation process.

Overall, the results of this study demonstrate that the electrooxidation of glycidol on polycrystalline gold electrodes follows a complex mechanism that involves carbon–carbon bond cleavage and the formation of multiple oxidation intermediates. The primary products identified by FTIR spectroscopy include formate, carbonate, and glycolic acid, as well as the signal associated with the CO_2 formation, which only appears at high applied potentials due to some local pH distortion. In contrast, the main products identified from the electrooxidation of glycerol on a gold electrode also include glyceric acid, besides glycolic and formic acids [37,52].

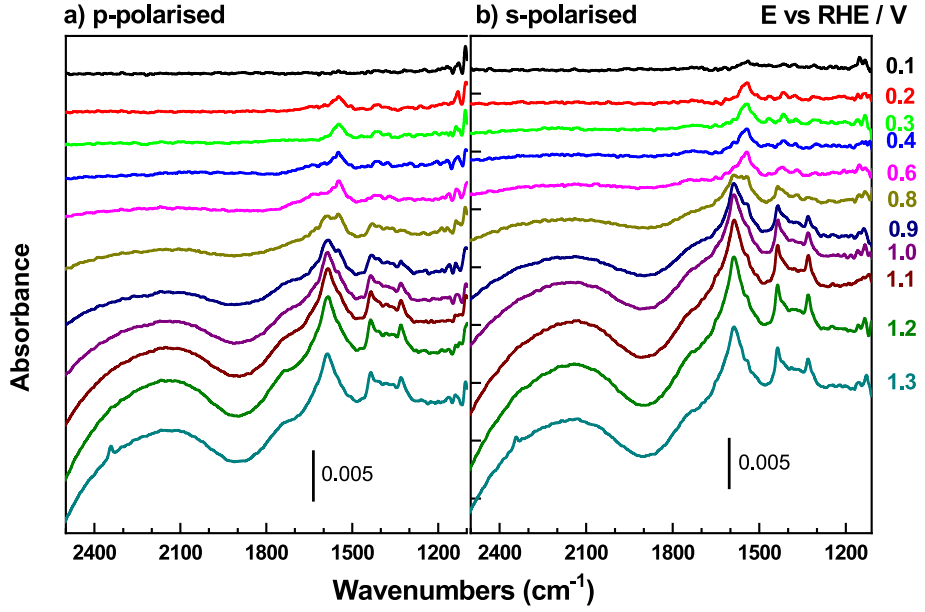

Fig. 9. In situ IRRAS spectra ((a) p-polarization) and ((b) s-polarization) for the electrooxidation of glycidol on a gold electrode in 0.10 M NaOH +0.10 M glycidol. (For interpretation of the references to colour in this figure legend, the reader is referred to the web version of this article.)

4. Conclusions

The electrochemical oxidation of a renewable glycerol-derived platform molecule, namely glycidol, was studied for the first time on gold electrodes using cyclic voltammetry, chronoamperometry and IR spectroscopy. Glycidol and glycerol electrooxidation reactions were analyzed and compared in both alkaline and acidic media. Both studied alcohols exhibited high reactivity in alkaline conditions, with glycerol exhibiting approximately three times more oxidation current than glycidol at the peak potential from cyclic voltammetry. This difference in reactivity can be attributed to the presence of the epoxy group in glycidol and, more importantly, to the lower acidity of glycidol's hydroxyl group compared to glycerol. Therefore, the deprotonation of the α-hydroxy group in glycidol appears to be a crucial step in its oxidation mechanism. Under acidic conditions, the reactivity of both glycerol and glycidol was significantly lower than in alkaline media, but with similar oxidation behavior for both molecules. These results suggest that oxidation activation is strongly dependent on the presence of hydroxyl groups, which are more abundant in the case of glycerol than in glycidol. The electrooxidation process leads to the cleavage of the glycidol C—C bonds, resulting in the formation of various carboxylic acids and CO_2, as demonstrated by in situ IRRAS experiments. Among the oxidation products, formate, carbonate, and glycolic acid were identified in solution, confirming the complete fragmentation of the glycidol molecule during electrooxidation. Overall, these results indicate that protected forms of glycerol, such as glycidol, are generally more resistant towards electrochemical oxidation. However, despite its lower reactivity compared to glycerol, glycidol oxidation on gold in alkaline media still represents an interesting molecule for more sustainable fuel cell applications. With its low viscosity, renewable origin, wide accessibility, and improved handling and storage properties, glycidol could serve as a viable alternative biofuel, contributing to the valorization of glycerol and their derived compounds, as well as to the development of more sustainable energy and electrochemical technologies.

CRediT authorship contribution statement

Dalila S. Mekazni: Investigation, Data curation. **Antonio Rodes:** Writing – review & editing, Investigation, Data curation. **Rosa M. Arán-Ais:** Writing – review & editing, Supervision. **Alejandro Leal-Duaso:** Writing – review & editing, Writing – original draft, Supervision, Investigation, Funding acquisition, Formal analysis, Data curation, Conceptualization. **Carlos M. Sánchez-Sánchez:** Writing – review & editing, Supervision, Funding acquisition, Formal analysis. **Enrique Herrero:** Writing – review & editing, Validation, Supervision, Funding acquisition, Formal analysis.

Declaration of competing interest

The authors declare that they have no known competing financial interests or personal relationships that could have appeared to influence the work reported in this paper.

Acknowledgements

This research was funded by Ministerio de Ciencia, Innovación y Universidades (Spain) grant numbers PID2022-137350NB-I00 and PID2021-125762NB-I00, and by the Centre National de la Recherche Scientifique (CNRS). D.S. Mekazni thanks the Government of Argelia for the award of a doctoral fellowship to support her studies at the University of Alicante (Spain). A. Leal-Duaso acknowledges the "Programa Margarita Salas 2021–2023" (Plan Nacional de Recuperación, Transformación y Resiliencia) financed by the "European Union-NextGenerationEU Program through the Ministerio de Universidades of Spain and the University of Zaragoza".

References

[1] N.A.A. Qasem, G.A.Q. Abdulrahman, A recent comprehensive review of fuel cells: history, types, and applications, Int. J. Energy Res. 2024 (2024) 7271748, https://doi.org/10.1155/2024/7271748.
[2] M.M. Tellez-Cruz, J. Escorihuela, O. Solorza-Feria, V. Compañ, Proton exchange membrane fuel cells (PEMFCs): advances and challenges, Polymers 13 (2021) 3064, https://doi.org/10.3390/polym13183064.
[3] X. Zhang, S.H. Chan, G. Li, H.K. Ho, J. Li, Z. Feng, A review of integration strategies for solid oxide fuel cells, J. Power Sources 195 (2010) 685–702, https://doi.org/10.1016/j.jpowsour.2009.07.045.
[4] I. Sebbani, M.K. Ettouhami, M. Boulakhbar, Fuel cells: a technical, environmental, and economic outlook, Clean. Energy Syst. 10 (2025) 100168, https://doi.org/10.1016/j.cles.2024.100168.
[5] C.A. Martínez-Huitle, M.A. Rodrigo, I. Sirés, O. Scialdone, A critical review on latest innovations and future challenges of electrochemical technology for the abatement of organics in water, Appl. Catal. B Environ. 328 (2023) 122430, https://doi.org/10.1016/j.apcatb.2023.122430.
[6] A. Leal-Duaso, L. Salvatella, J.M. Fraile, Physical-chemical transformations for the remediation and valorization of hexachlorocyclohexanes (HCHs) including lindane: a review, J. Environ. Manag. 375 (2025) 124262–124300, https://doi.org/10.1016/j.jenvman.2025.124262.
[7] S.-G. Sun, Y. Lin, Kinetics of isopropanol oxidation on Pt(111), Pt(110), Pt(100), Pt (610) and Pt(211) single crystal electrodes - studies of in situ time-resolved FTIR spectroscopy, Electrochim. Acta 44 (1998) 1153–1162, https://doi.org/10.1016/S0013-4686(98)00218-7.
[8] I.A. Rodrigues, F.C. Nart, 2-propanol oxidation on platinum and platinum–rhodium electrodeposits, J. Electroanal. Chem. 590 (2006) 145–151, https://doi.org/10.1016/j.jelechem.2006.02.030.
[9] A. Sáez, E. Expósito, J. Solla-Gullón, V. Montiel, A. Aldaz, Bismuth-modified carbon supported Pt nanoparticles as electrocatalysts for direct formic acid fuel cells, Electrochim. Acta 63 (2012) 105–111, https://doi.org/10.1016/j.electacta.2011.12.076.
[10] J. Chang, L. Feng, C. Liu, W. Xing, X. Hu, An effective Pd-Ni(2)P/C anode catalyst for direct formic acid fuel cells, Angew. Chem. Int. Ed. Eng. 53 (2014) 122–126, https://doi.org/10.1002/anie.201308620.
[11] J.V. Perales-Rondón, E. Herrero, J. Solla-Gullón, C.M. Sánchez-Sánchez, V. Vivier, Oxygen crossover effect on palladium and platinum based electrocatalysts during formic acid oxidation studied by scanning electrochemical microscopy, J. Electroanal. Chem. 793 (2017) 218–225, https://doi.org/10.1016/j.jelechem.2016.12.049.
[12] T. Uda, D.A. Boysen, C.R.I. Chisholm, S.M. Haile, Alcohol fuel cells at optimal temperatures, Electrochem. Solid-State Lett. 9 (2006) A261, https://doi.org/10.1149/1.2188069.
[13] A. Santasalo, F.J. Vidal-Iglesias, J. Solla-Gullón, A. Berná, T. Kallio, J.M. Feliu, Electrooxidation of methanol and 2-propanol mixtures at platinum single crystal electrodes, Electrochim. Acta 54 (2009) 6576–6583, https://doi.org/10.1016/j.electacta.2009.06.033.
[14] M.C. Figueiredo, A. Santasalo-Aarnio, F.J. Vidal-Iglesias, J. Solla-Gullón, J. M. Feliu, K. Kontturi, T. Kallio, Tailoring properties of platinum supported catalysts by irreversible adsorbed adatoms toward ethanol oxidation for direct ethanol fuel cells, Appl. Catal. B Environ. 140–141 (2013) 378–385, https://doi.org/10.1016/j.apcatb.2013.04.038.
[15] G. Melle, M.B.C. De Souza, P.V.B. Santiago, P.G. Corradini, L.H. Mascaro, P. S. Fernández, E. Sitta, Glycerol electro-oxidation at Pt in alkaline media: influence of mass transport and cations, Electrochim. Acta 398 (2021) 139318, https://doi.org/10.1016/j.electacta.2021.139318.
[16] V. Del Colle, G. Melle, B.A.F. Previdello, J.M. Feliu, H. Varela, G. Tremiliosi-Filho, The effect of Pt surface orientation on the oscillatory electro-oxidation of glycerol, J. Electroanal. Chem. 926 (2022) 116934, https://doi.org/10.1016/j.jelechem.2022.116934.
[17] J. Brouwer, On the role of fuel cells and hydrogen in a more sustainable and renewable energy future, Curr. Appl. Phys. 10 (2010) S9–S17, https://doi.org/10.1016/j.cap.2009.11.002.
[18] R. Ciriminna, C.D. Pina, M. Rossi, M. Pagliaro, Understanding the glycerol market, Eur. J. Lipid Sci. Technol. 116 (2014) 1432–1439, https://doi.org/10.1002/ejlt.201400229.
[19] J.I. García, H. García-Marín, E. Pires, Glycerol based solvents: synthesis, properties and applications, Green Chem. 16 (2014) 1007–1033, https://doi.org/10.1039/C3GC41857J.
[20] A. Leal-Duaso, I. Favier, D. Pla, E. Pires, M. Gómez, Design of glycerol-based solvents for the immobilization of palladium nanocatalysts: a hydrogenation study, ACS Sustain. Chem. Eng. 9 (2021) 6875–6885, https://doi.org/10.1021/acssuschemeng.1c01694.
[21] S. Velasco-Lozano, M. Roca, A. Leal-Duaso, J.A. Mayoral, E. Pires, V. Moliner, F. López-Gallego, Selective oxidation of alkyl and aryl glyceryl monoethers catalysed by an engineered and immobilised glycerol dehydrogenase, Chem. Sci. 11 (2020) 12009–12020, https://doi.org/10.1039/d0sc04471g.
[22] P. Prete, D. Cespi, F. Passarini, C. Capacchione, A. Proto, R. Cucciniello, Glycidol syntheses and valorizations: boosting the glycerol biorefinery, Curr. Opin. Green Sustain. Chem. 35 (2022) 100624, https://doi.org/10.1016/j.cogsc.2022.100624.
[23] A. Leal-Duaso, P. Pérez, J.A. Mayoral, E. Pires, J.I. García, Glycerol as a source of designer solvents: physicochemical properties of low melting mixtures containing glycerol ethers and ammonium salts, Phys. Chem. Chem. Phys. 19 (2017) 28302–28312, https://doi.org/10.1039/C7CP04987K.

[24] E. Pires, J.I. García, A. Leal-Duaso, J.A. Mayoral, J.I. García-Peiro, D. Velázquez, Optimization of the synthesis of glycerol derived Monoethers from Glycidol by means of heterogeneous acid catalysis, Molecules 23 (2018) 2887–2996, https://doi.org/10.3390/molecules23112887.
[25] A. Leal-Duaso, M. Caballero, A. Urriolabeitia, J.A. Mayoral, J.I. García, E. Pires, Synthesis of 3-alkoxypropan-1,2-diols from glycidol: experimental and theoretical studies for the optimization of the synthesis of glycerol derived solvents, Green Chem. 19 (2017) 4176–4185, https://doi.org/10.1039/C7GC01583F.
[26] A. Leal-Duaso, P. Pérez, J.A. Mayoral, J.I. García, E. Pires, Glycerol-derived solvents: synthesis and properties of symmetric glyceryl diethers, ACS Sustain. Chem. Eng. 7 (2019) 13004–13014, https://doi.org/10.1021/acssuschemeng.9b02105.
[27] A. Leal-Duaso, S. Gracia-Barberán, J.A. Mayoral, J.I. García, E. Pires, Readily scalable methodology for the synthesis of nonsymmetric glyceryl Diethers by a tandem acid-/base-catalyzed process, Org. Process. Res. Dev. 24 (2020) 154–162, https://doi.org/10.1021/acs.oprd.9b00411.
[28] M.P. Garralaga, L. Lomba, A. Leal-Duaso, S. Gracia-Barberán, E. Pires, B. Giner, Ecotoxicological study of bio-based deep eutectic solvents formed by glycerol derivatives in two aquatic biomodels, Green Chem. 24 (2022) 5228–5241, https://doi.org/10.1039/D2GC01293F.
[29] M. Valter, M. Busch, B. Wickman, H. Grönbeck, J. Baltrusaitis, A. Hellman, Electrooxidation of glycerol on gold in acidic medium: a combined experimental and DFT study, J. Phys. Chem. C 122 (2018) 10489–10494, https://doi.org/10.1021/acs.jpcc.8b02685.
[30] M. Braun, C.S. Santana, A.C. Garcia, C. Andronescu, From waste to value – glycerol electrooxidation for energy conversion and chemical production, Curr. Opin. Green Sustain. Chem. 41 (2023) 100829, https://doi.org/10.1016/j.cogsc.2023.100829.
[31] J. Wu, X. Yang, M. Gong, Recent advances in glycerol valorization via electrooxidation: catalyst, mechanism and device, Chin. J. Catal. 43 (2022) 2966–2986, https://doi.org/10.1016/S1872-2067(22)64121-4.
[32] R.M.L.M. Sandrini, J.R. Sempionatto, G. Tremiliosi-Filho, E. Herrero, J.M. Feliu, J. Souza-Garcia, C.A. Angelucci, Electrocatalytic oxidation of glycerol on platinum single crystals in alkaline media, ChemElectroChem 6 (2019) 4238–4245, https://doi.org/10.1002/celc.201900311.
[33] C. Coutanceau, S. Baranton, R.S.B. Kouamé, Selective electrooxidation of glycerol into value-added chemicals: a short overview, Front. Chem. 7 (2019) 1–15, https://doi.org/10.3389/fchem.2019.00100.
[34] M. Guschakowski, U. Schröder, Direct and indirect Electrooxidation of glycerol to value-added products, ChemSusChem 14 (2021) 5216–5225, https://doi.org/10.1002/cssc.202100556.
[35] H. Inoue, S. Kimura, Y. Teraoka, M. Chiku, E. Higuchi, B.T.X. Lam, Mechanism of glycerol oxidation reaction on silver-modified palladium electrode in alkaline medium, Int. J. Hydrog. Energy 43 (2018) 18664–18671, https://doi.org/10.1016/j.ijhydene.2018.05.076.
[36] J. Zhang, Y. Liang, N. Li, Z. Li, C. Xu, S.P. Jiang, A remarkable activity of glycerol electrooxidation on gold in alkaline medium, Electrochim. Acta 59 (2012) 156–159, https://doi.org/10.1016/j.electacta.2011.10.048.
[37] L. Pérez-Martínez, L. Balke, A. Cuesta, Reactive and inhibiting species in the electrocatalytic oxidation of glycerol on gold. A study combining in-situ visible reflectance and ATR-SEIRAS, J. Catal. 394 (2021) 1–7, https://doi.org/10.1016/j.jcat.2020.12.010.
[38] T. Andreu, M. Mallafré, M. Molera, M. Sarret, R. Oriol, I. Sirés, Effect of thermal treatment on nickel-cobalt electrocatalysts for glycerol oxidation, ChemElectroChem 9 (2022) e202200100, https://doi.org/10.1002/celc.202200100.
[39] C.A. Angelucci, J. Souza-Garcia, P.S. Fernández, P.V.B. Santiago, R.M.L. M. Sandrini, Glycerol electrooxidation on noble metal electrode surfaces, Encyclopedia Interfacial Chem.: Surface Sci. Electrochem. (2018) 643–650, https://doi.org/10.1016/B978-0-12-409547-2.13330-X.
[40] G.A.B. Mello, C. Busó-Rogero, E. Herrero, J.M. Feliu, Glycerol electrooxidation on Pd modified au surfaces in alkaline media: effect of the deposition method, J. Chem. Phys. 150 (2018) 041703, https://doi.org/10.1063/1.5048489.
[41] M. Simões, S. Baranton, C. Coutanceau, Electro-oxidation of glycerol at Pd based nano-catalysts for an application in alkaline fuel cells for chemicals and energy cogeneration, Appl. Catal. B Environ. 93 (2010) 354–362, https://doi.org/10.1016/j.apcatb.2009.10.008.
[42] T. Li, D.A. Harrington, An overview of glycerol Electrooxidation mechanisms on Pt, Pd and au, ChemSusChem 14 (2021) 1472–1495, https://doi.org/10.1002/cssc.202002669.
[43] D.S. Mekazni, R.M. Arán-Ais, A. Ferre-Vilaplana, E. Herrero, Why methanol electro-oxidation on platinum in water takes place only in the presence of adsorbed OH, ACS Catal. 12 (2022) 1965–1970, https://doi.org/10.1021/acscatal.1c05122.
[44] R. Rizo, A. Ferre-Vilaplana, E. Herrero, J.M. Feliu, Ethanol electro-oxidation reaction selectivity on platinum in aqueous media, ACS Sustain. Chem. Eng. 11 (2023) 4960–4968, https://doi.org/10.1021/acssuschemeng.2c02663.
[45] Y. Kwon, S.C.S. Lai, P. Rodriguez, M.T.M. Koper, Electrocatalytic oxidation of alcohols on gold in alkaline media: base or gold catalysis? J. Am. Chem. Soc. 133 (2011) 6914–6917, https://doi.org/10.1021/ja200976j.
[46] X. Shi, D.E. Simpson, D. Roy, The role of chemisorbed hydroxyl species in alkaline electrocatalysis of glycerol on gold, Phys. Chem. Chem. Phys. 17 (2015) 11432–11444, https://doi.org/10.1039/C5CP00313J.
[47] G. Nikolic, S. Zlatkovic, M. Cakic, S. Cakic, C. Lacnjevac, Z. Rajic, Fast fourier transform IR characterization of epoxy GY systems crosslinked with aliphatic and cycloaliphatic EH polyamine adducts, Sensors 10 (2010) 684–696, https://doi.org/10.3390/s100100684.
[48] J.F. Gomes, G. Tremiliosi-Filho, Spectroscopic studies of the glycerol electro-oxidation on polycrystalline au and Pt surfaces in acidic and alkaline media, Electrocatalysis 2 (2011) 96–105, https://doi.org/10.1007/s12678-011-0039-0.
[49] G. Socrates, Infrared and Raman Characteristic Group Frequencies: Tables and Charts, 3rd edition, Wiley, Chichester, 2004.
[50] J.M. Delgado, R. Blanco, J.M. Orts, J.M. Pérez, A. Rodes, Glycolate adsorption at gold and platinum electrodes: a theoretical and in situ spectroelectrochemical study, Electrochim. Acta 55 (2010) 2055–2064, https://doi.org/10.1016/j.electacta.2009.11.034.
[51] P.-O. Morisset, J. Gagnon, R. Tremblay, J.-S. Deschênes, Development and validation of an in situ and real-time quantification method for bicarbonate, carbonate and orthophosphate ions by ATR FT-IR spectroscopy in aqueous solutions, Analyst 143 (2018) 4387–4393, https://doi.org/10.1039/C8AN00687C.
[52] Y. Kwon, M.T.M. Koper, Combining voltammetry with HPLC: application to electro-oxidation of glycerol, Anal. Chem. 82 (2010) 5420–5424, https://doi.org/10.1021/ac101058t.